Model calculations of the quantum ballistic transport in two-dimensional constriction-type microstructures

D. van der Marel and E. G. Haanappel
Faculty of Applied Physics, Delft University of Technology, Lorentzweg 1, 2628 CJ Delft, The Netherlands
(Received 20 October 1988)

We describe an exact formalism for the calculation of the zero-temperature dc conductance of various constriction-type microstructures connected to a two-dimensional half plane on both sides. From our results we obtain quantized conductance as a function of constriction width at integer multiples of $2e^2/h$ for constrictions shorter than a Fermi wavelength. For longer constrictions, the conductance oscillates below the quantized values. The effect of impurities is to destroy quantization if the impurities are within a few wavelengths of the aperture. We show that there is a weak diffraction pattern in the transmitted electronic amplitude superimposed on the classical $\cos(\alpha)$ behavior.

I. INTRODUCTION

Recently much interest has been raised in the quantum ballistic transport properties of low-dimensional microstructures. In particular, the experimental observation by van Wees *et al.*[1] and by Wharam *et al.*,[2] that the conductance through a narrow constriction defined with a split gate in a GaAs/$Al_xGa_{1-x}As$ two-dimensional (2D) electron gas increases with steps of $2e^2/h$ on increasing the constriction width, has stimulated the discussion concerning the nature of coherent electron transport. In the discussion of ballistic conductance in mesoscopic structures the Landauer-type formula $G=(e^2/h)\mathrm{Tr}(t^\dagger t)$ plays a central role. This formula, which is a multichannel version of a strictly 1D formula originally proposed by Landauer,[3] has been derived in various ways[4–6] and forms the basis of many calculations of the conductance in ultrasmall metallic samples. Recently we proposed a model[7] for the conductance of 2D Sharvin point contacts, which is strongly related to the Landauer type of approach, without, however, making explicit use of the transmission matrix t. Instead we used a T-matrix approach, which reduces the problem to a numerical matrix inversion involving only the sites of the aperture and additional impurities. In this paper we present a complete and also extended version of the theory underlying Ref. 7. The extension of the theory allows us to study conductance in a wide variety of constriction-type geometries, where the constriction region is flanked by true 2D halfplanes. Our model is based on a tight-binding description of the electronic states and is fully rigorous regardless of which part of the Brillouin zone the Fermi surface is located in. One of the advantages of the tight-binding method is that the problem is automatically discretized. In models based on free-electron wave functions a discretization stage has to be introduced at some point at the expense of rigor. Another advantage is that one avoids the ultraviolet divergencies occurring in the diagonal elements of free-electron Green's functions. This is due to the high-energy cutoff in the density of states intrinsic to a tight-binding band.

Calculations of conductance based on tight-binding schemes have been established by Lee and Fisher[8] in the context of Anderson localization in two dimensions and by Stone[9] for the calculation of the magnetoresistance of wires and rings. These approaches are based on the multichannel version of the Landauer formula. The conductance is calculated over a disordered region connected on both sides to channels of infinite length and with a finite width. Due to their finite width, the transverse momentum of the connecting wires is quantized and each of these quantized momenta corresponds to a 1D subband or "channel." The applicability of these methods to constrictions flanked by 2D regions is limited, due to the fact that the perturbation potential includes the (infinite) barrier itself. A realistic calculation where the length of the barrier exceeds the constriction size by at least an order of magnitude, involves a matrix inversion of the huge number of points. It is for this reason that we map the problem onto the limited set of points of the perturbation potential inside and near the aperture.

We will apply our model calculations to the problem of the conductance of constrictions as a function of width in the spirit of the experiments by van Wees *et al.*[1] and Wharam *et al.*[2] In these experiments it was found that the two-terminal conductance over a narrow constriction in a 2D electron gas rises in a stepwise fashion with plateaux at integer multiples of $2e^2/h$. Although this stepwise rise was nowhere mentioned in the literature before the experiments were reported, it has been anticipated by Imry,[10] Büttiker,[11] and Landauer[4] that a quantized contact resistance exists between a one-dimensional channel and a reservoir. Van Gelder[12] and Garcia[13] anticipated oscillating behavior of the conductance as a function of the tip size of a scanning tunneling microscope, but without quantization at multiples of $2e^2/h$.

One of the important questions is how general this type of conductance quantization is. It is particularly interest-

ing to know how stable the quantization is against sample imperfections. As this quantization involves no magnetic field it could—at least in principle—be an interesting alternative for the quantum Hall effect as a basis for a resistance standard. In Ref. 7 we have already shown that the quantization occurring in short constrictions is strongly distorted by impurities in the aperture region. With the extended formalism presented here, we will show that in the case of a constriction of finite length (which is closer to usual experimental conditions) the quantization is also strongly influenced by impurities at a distance of the order of a wavelength from the aperture. We find that the formation of horizontal plateaux evolves rapidly as a function of increasing channel length. The plateaux are fully developed for a constriction length of the order of a Fermi wavelength.

In our approach we first derive analytical expressions for the Green's functions and the wave functions of the Hamiltonian of a 2D plane with a closed barrier of finite height V. In the next step we take away part of the barrier by adding a potential $-V$ to a limited set of lattice points on the barrier. We also put a potential V on a limited set of lattice points in the plane, which may be arranged in the shape of a tube or some other microstructure. In Fig. 1 the arrangement of the various terms of the potential landscape is displayed. We then calculate the T matrix due to the presence of the orifice and the additional number of lattice points of the localized perturbation potential. This part of the method is strongly related to the recent work by Lucas *et al.*[14] on the scanning tunneling microscope. There are two important differences with their work. (1) We take the simplest model for the barrier part, which allows us to calculate the zeroth-order wave functions as well as the Green's functions analytically. (2) Our results are fully rigorous for all values of the mesh due to the use of a tight-binding Hamiltonian. We finally derive a rather simple analytical expression relating the conductance to the T matrix and the Green's function of the closed-barrier Hamiltonian, which can be fed into a computer.

In our theory we can vary the following parameters: (1) the Fermi energy, (2) the lattice parameter, and (3) the shape and size of the localized perturbation potential. If we choose the lattice parameter small with respect to the Fermi wavelength, we are in the free-electron limit. On the other hand, if we choose a large Fermi wave vector we are in the metallic regime, where the Fermi surface becomes anisotropic. The remaining sections are organized as follows. In Sec. II we describe how the Landauer formula can be written in terms of a Fermi average over the flux carried by the wave functions and we derive an expression for the flux in terms of those wave functions in the case of a tight-binding Hamiltonian. In Sec. III we derive analytical expressions for the Green's functions and the wave functions corresponding to the barrier Hamiltonian, which we consider as the unperturbed Hamiltonian throughout this paper. In Sec. IV we derive analytical expressions for the T matrix of the total Hamiltonian and we derive the final expressions for the conductance. In Sec. V we discuss numerical examples of our method and relate them to the experiments.[1,2]

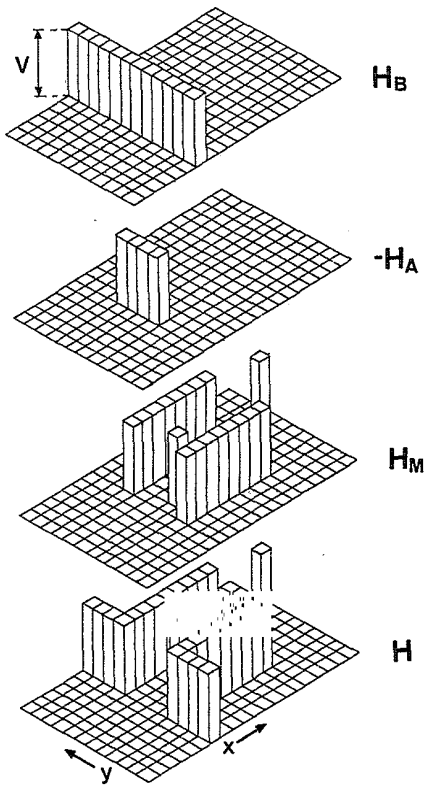

FIG. 1. The potential landscape for which we calculate the conductance. Indicated are the barrier part (H_B), the aperture part ($-H_A$), the microstructure part (H_M), and the total Hamiltonian (H).

II. EXPRESSIONS FOR THE CONDUCTANCE

Although there has been quite some discussion in the past about which version of the Landauer equation is applicable,[15] it is now generally agreed that the ballistic *two-terminal* conductance through a region acting as a barrier is given by

$$G=\frac{e^2}{h}\mathrm{Tr}(t^\dagger t)\ , \tag{1}$$

where t is the transmission matrix and the trace includes the spin degeneracy. The general acceptance of the latter formula in the case of two terminals only is mainly due to the work of Imry[10] and Büttiker.[11] The physical meaning of the trace over the transmission matrix is that it represents a sum over states at the Fermi level of the probability density carried from one side of the barrier to the other per unit of time. Throughout this paper we will use the convention that net flux flows from left to right, i.e., the electrical current flows from right to left. We can replace the summation over states at the Fermi level with a weighted angular integration, where the weight is given by the density of k states per unit angle and per unit energy. The resulting expression is

$$G=e^2\int_{-\pi/2}^{\pi/2}\Phi(E_F,\alpha)\frac{\partial^2 n}{\partial E\,\partial\alpha}d\alpha\ . \tag{2}$$

Here the flux $\Phi(E_F,\alpha)$ is the rate at which a unit area corresponding to an eigenstate $|\Phi_\alpha\rangle$ at the Fermi surface crosses the constriction. Far away from the constriction the eigenstates are characterized by the angle of incidence α. The term $\partial^2 n/\partial E\partial\alpha$ represents the spin-degenerate density of states per unit area and per unit angle, which can in principle depend on α. Equations (1) and (2) presume the presence of randomizing baths on both sides of the region where the conductance is calculated. Even in the absence of elastic scattering we find a finite flux which is proportional to the sample width, so that the conductance remains finite. According to Imry[10] this has to be interpreted as a contact resistance between the reservoir and the ballistic part of the sample and it is a consequence of the fact that current is carried by particles with a finite (Fermi) velocity. This is also the origin of the finite Sharvin resistance[16–18] of classical ballistic particles in a point contact.

The flux of each eigenstate can be calculated by acting with the time derivative operator on $|\psi|^2$ and by employing the time-dependent Schrödinger equation. The eigenstate ψ has to be split in a left-hand and a right-hand part, $\psi=\psi_L+\psi_R$, so that the flux from the set of points at the left side L to the set of points at the right side R follows from[19]

$$\Phi(\psi)=\frac{i}{\hbar}\int_{r\in L}[\psi_L^*(r)\langle r|H|\psi_R\rangle-\psi_L(r)\langle\psi_R|H|r\rangle]d^2r\ . \tag{3}$$

In Sec. III we introduce a tight-binding Hamiltonian with nearest-neighbor coupling, the hopping part of which is

$$H_0=4t\left[1-\tfrac{1}{4}\sum_{m,n}|m,n\rangle\langle m\pm1,n\pm1|\right]\ .$$

As we consider the case of a constriction in a barrier, a convenient choice of L is the set of sites at the left side of the barrier including the barrier itself. We note that the only nonzero terms in the summation of Eq. (3) come from the set of points at the dividing line ($m=0$), so that Eq. (3) reduces to

$$\Phi(\psi)=\frac{4\pi ta^2}{h}\mathrm{Im}\left[\sum_{n\in A}\langle\psi|0,n\rangle\langle 1,n|\psi\rangle\right]\ . \tag{4}$$

Here A is the set of sites constituting the aperture and t is the hopping parameter.

III. SOLUTION OF THE BARRIER HAMILTONIAN

In this section we calculate wave functions $|\phi\rangle$ and the Green's functions G for a 2D tight-binding Hamiltonian containing a 1D barrier potential with height V. The Hamiltonian that we will use is

$$H=H_B+H_L\ . \tag{5}$$

We will discuss the localized part H_L in the following section. The barrier part H_B consists of the tight-binding Hamiltonian H_0, which is translationally invariant in both directions, and the barrier potential H_1, which has translational symmetry in the y direction. The tight-binding wave functions form a 2D square lattice with lattice spacing a. The choice of parameters in H_0 is such that it corresponds to the free-electron Hamiltonian in the long-wavelength limit. The effective mass equals $\hbar^2/(2ta^2)$ in this part of the Brillouin zone. The barrier Hamiltonian is

$$\begin{aligned}H_B&=H_0+H_1\ ,\\ H_0&=4t\left[1-\tfrac{1}{4}\sum_{m,n}|m,n\rangle\langle m\pm1,n\pm1|\right]\ ,\\ H_1&=V\sum_n|0,n\rangle\langle 0,n|\ .\end{aligned} \tag{6}$$

The wave functions of H_B are easily obtained by solving the Schrödinger equation and are presented here for later reference. Our notation for the projection operators is as follows: We use $|k\rangle$, $|\phi_k\rangle$, and $|\psi_k\rangle$ to indicate the eigenstates of H_0, H_B, and H, respectively. It is a textbook exercise to derive that for $k_x>0$

$$|\phi_k\rangle=|k_L\rangle+\frac{1}{V+2it\sin(k_xa)}\times[-V|-k_L\rangle+2it\sin(k_xa)|k_R\rangle]\ . \tag{7}$$

Here $|k_L\rangle$ and $|k_R\rangle$ are the projections of $|k\rangle$ on the left half-plane and the right half-plane:

$$\begin{aligned}|k_L\rangle&=\sum_{m\le0}e^{i(k_xam+k_yan)}|m,n\rangle\ ,\\ |k_R\rangle&=\sum_{m\ge1}e^{i(k_xam+k_yan)}|m,n\rangle\ .\end{aligned} \tag{8}$$

For $k_x<0$ the eigenstates of H_B are the mirror images of Eq. (7). The eigenstates of H_0 are normalized on a unit square. The states of Eq. (7) form an orthonormal set and represent left-side and right-side lobes, which correspond to standing waves at the left and the right side of the barrier in the limit of an infinite-barrier potential. The set of states represented by Eq. (7) is not complete. There are also bound states located at the barrier, with energies approximately equal to the barrier potential. These states can be disregarded in the present discussion, as we are only interested in the current-carrying states. The energies of the continuum states of H_B are equal to those of H_0:

$$E(\phi_k)=E(k)=2t[2-\cos(k_xa)-\cos(k_ya)]\ . \tag{9}$$

The next step is to derive the expressions for the Green's functions of H_B. As we have already done for the calculation of the wave functions, we can take advantage of the fact that H_B has translational symmetry in the y direction by using momentum coordinates for the y direction and direct space coordinates for the x direction. In this representation the Green's function of H_0 is, following Economou,[20]

$$g(m,k_y;m',k_y)=\frac{1}{2t}\frac{[(\zeta^2-1)^{1/2}-\zeta]^{|m-m'|}}{(\zeta^2-1)^{1/2}}\ , \tag{10}$$

where we defined $\zeta\equiv E/2t-2+\cos(k_ya)$. The Green's function G corresponding to H_B is now obtained from the

Dyson equation relating G to g and H_1:

$$G(m,k_y;m',ky)=g(m,k_y;m',k_y)+g(m,k_y;0,k_y)VG(0,k_y;m',k_y)$$

which immediately leads to

$$G(m;m')=g(m;m')-\frac{g(m;0)g(0;m')}{g(0;0)}\times\left[1+\frac{1}{Vg(0;0)}+\left[\frac{1}{Vg(0;0)}\right]^2+\cdots\right]. \quad (11)$$

We dropped the repeated index k_y for brevity. We take the limit of infinite V in the final expressions, so that we only need the leading orders in $1/V$. G is easily obtained in real-space representation by means of a Fourier transformation of Eq. (11) over k_y. Note that for $m=0$ or $m'=0$ the first two terms in Eq. (11) cancel. Moreover, it will turn out that for $m=m'=0$ we will need the leading term as well as the second term, due to cancellation of the former in the expressions for the T matrix. We therefore have to consider the three following cases: (1) $m=m'=0$, (2) $m=0$ and $m'\neq 0$, and (3) $m\neq 0$ and $m'\neq 0$, for which we find, respectively,

$$G(0,n;0,n')=-\frac{1}{V}\delta_{n,n'}-\frac{2t}{V^2}\gamma(n-n')+O(V^{-3}),$$

$$G(0,n;m',n')=-\frac{1}{V}\omega(m',n-n')+O(V^{-2}), \quad (12)$$

$$G(m,n;m',n')=\frac{1}{2t}\lambda(m,m',n-n')+O(V^{-1}).$$

Here we introduce the following functions, with the substitution $\phi=k_y a$:

$$\gamma(n)\equiv\pi^{-1}\int_0^{\pi}(\xi^2-1)^{1/2}\cos(n\phi)d\phi, \quad (13a)$$

$$\omega(m,n)\equiv\pi^{-1}\int_0^{\pi}[(\xi^2-1)^{1/2}-\xi]^{|m|}\cos(n\phi)d\phi, \quad (13b)$$

$$\lambda(m,m',n)\equiv\pi^{-1}\int_0^{\pi}\frac{[(\xi^2-1)^{1/2}-\xi]^{|m-m'|}-[(\xi^2-1)^{1/2}-\xi]^{|m+m'|}}{(\xi^2-1)^{1/2}}\cos(n\phi)d\phi. \quad (13c)$$

In the next section the following identities will turn out to be useful:

$$\omega(1,n-n')=\gamma(n-n')-\left[\frac{E}{2t}-2\right]\delta_{n,n'}-\tfrac{1}{2}\delta_{1,|n-n'|}, \quad (14a)$$

$$\lambda(m,1,n-n')=-2\omega(m,n-n'). \quad (14b)$$

IV. SOLUTION OF THE FULL HAMILTONIAN

The localized part of the Hamiltonian (H_L) consists of two terms. The first term (H_A) removes a finite part of the barrier potential, as discussed in the preceding section. It does not make any difference in our analysis how this part is distributed over the barrier. We define a set of points A with x coordinate $m_x=0$ as the set of points constituting the aperture(s) which can in principle also contain delta-function impurities. The second term of H_L, which we will indicate as the microstructure Hamiltonian H_M, is a set of delta-function potentials representing any convenient shape in the 2D plane. The total Hamiltonian to be solved is

$$H=H_B+H_A+H_M. \quad (15)$$

The barrier Hamiltonian H_B was discussed in the previous section. The aperture Hamiltonian is

$$H_A=-V\sum_{n\in A}|0,n\rangle\langle 0,n|. \quad (16)$$

Here A is some set of points spread over the barrier, which represents a single- or multiple-slit configuration. A delta-function impurity located inside the aperture is incorporated by excluding a site from the row of sites representing the aperture. The perturbation Hamiltonian H_M is

$$H_M=V\sum_{(m,n)\in M}|m,n\rangle\langle m,n|. \quad (17)$$

This set of points, can, for example, be used to define a pipe, fitted to the right side of the aperture A. We will use it to study the influence of the length of a constriction on its conductance, but other geometries can be studied equally well with the present formalism. We can obtain the T matrix from inversion of the T-matrix Dyson equation,[20]

$$\underline{T}[\underline{1}-\underline{G}(\underline{H}_A+\underline{H}_M)]=\underline{H}_A+\underline{H}_M. \quad (18)$$

As the indices A and M refer to two disjoint regions in 2D space, we can write Eq. (18) in matrix block form

$$\begin{bmatrix}\underline{T}_A^A & \underline{T}_A^M\\ \underline{T}_M^A & \underline{T}_M^M\end{bmatrix}\begin{bmatrix}-V\underline{1} & \underline{0}\\ \underline{0} & V\underline{1}\end{bmatrix}-\begin{bmatrix}\underline{G}_A^A & \underline{G}_A^M\\ \underline{G}_M^A & \underline{G}_M^M\end{bmatrix}\begin{bmatrix}-V\underline{1} & \underline{0}\\ \underline{0} & V\underline{1}\end{bmatrix}=\begin{bmatrix}-V\underline{1} & \underline{0}\\ \underline{0} & V\underline{1}\end{bmatrix} \quad (19)$$

or, using Eqs. (12)–(14),

$$\begin{bmatrix} \underline{T}^{A}_{A} & \underline{T}^{M}_{A} \\ \underline{T}^{A}_{M} & \underline{T}^{M}_{M} \end{bmatrix} \begin{bmatrix} \frac{2t}{V^2}\underline{\Gamma} & -\frac{1}{V}\underline{\Omega} \\ \frac{1}{V}\underline{\Omega}^{t} & \frac{1}{2T}\underline{\Lambda} \end{bmatrix} = \begin{bmatrix} \underline{1} & \underline{0} \\ \underline{0} & -\underline{1} \end{bmatrix} . \tag{20}$$

Here the matrix elements of $\underline{\Gamma}$, $\underline{\Omega}$, and $\underline{\Lambda}$ are given by the functions γ, ω, and λ defined in Eq. (14) for those sites which belong to the sets of A and M. The site indices m and n refer to x and y coordinates respectively,

$$\begin{aligned} &\Gamma^{j}_{i} \equiv \gamma(n_i - n_j) \quad (\underline{R}_i \in A,\ \underline{R}_j \in A) , \\ &\Omega^{j}_{i} \equiv \omega(m_j, n_j - n_i) \quad (\underline{R}_i \in A,\ \underline{R}_j \in M) , \\ &\Lambda^{j}_{i} \equiv \lambda(m_i, m_j, n_j - n_i) \quad (\underline{R}_i \in M,\ \underline{R}_j \in M) . \end{aligned} \tag{21}$$

We finally invert the block matrix Eq. (20) using standard matrix manipulation techniques and obtain, to leading order in $1/V$,

$$\begin{bmatrix} \underline{T}^{A}_{A} & \underline{T}^{M}_{A} \\ \underline{T}^{A}_{M} & \underline{T}^{M}_{M} \end{bmatrix} = \begin{bmatrix} \frac{V^2}{2t}\underline{\Theta} & V\underline{\Theta}\,\underline{\Omega}\,\underline{\Lambda}^{-1} \\ V\underline{\Lambda}^{-1}\underline{\Omega}^{t}\underline{\Theta} & -2t(\underline{\Omega}^{t}\underline{\Gamma}^{-1}\underline{\Omega} + \underline{\Lambda})^{-1} \end{bmatrix} , \tag{22}$$

$$\underline{\Theta} \equiv (\underline{\Gamma} + \underline{\Omega}\,\underline{\Lambda}^{-1}\underline{\Omega}^{t})^{-1} .$$

We can now combine our expressions for the T matrix with the Lippman-Schwinger equation in order to get the continuum states $|\psi_k\rangle$ of the total Hamiltonian defined in Eq. (15):

$$|\psi_k\rangle = |\phi_k\rangle + \underline{G}\,\underline{T}|\underline{\phi}_k\rangle . \tag{23}$$

This can be inserted into the expression for the flux, Eq. (4), which leads to the following relation between the flux and the T matrix:

$$\Phi(\psi_k) = \frac{4\pi t a^2}{h} \mathrm{Im} \sum_{n \in A} \langle \phi_k | \underline{T}^{\dagger} \underline{G}^{\dagger} | 0,n \rangle \langle 1,n | \underline{G}\,\underline{T} | \phi_k \rangle + O(V^{-1}) . \tag{24}$$

This equation is further evaluated by once again writing T and G in matrix block form and collecting leading orders in $1/V$, which is now $(1/V)^0$. We have to make a distinction here between the case where M includes only sites on the right side of the barrier and the more general case, where M includes sites on both sides. In the former case two nonvanishing terms contribute to Eq. (24), whereas in the latter case there are six additional terms. This is due to the fact that the wave functions $\langle m,n|\phi_k\rangle$ are of a different order in $1/V$ for (m,n) at the left and right sides of the barrier, as can be seen from Eq. (7). In the latter case we find for the flux

$$\Phi(\psi_k) = \frac{4\pi t a^2}{h} \mathrm{Im} \sum_{n \in A} \langle \phi_k | (\underline{T}^{A\dagger}_{A} + \underline{T}^{A\dagger}_{M}) \underline{G}^{\dagger} | 0,n \rangle \times \langle 1,n | \underline{G} (\underline{T}^{A}_{A} + \underline{T}^{M}_{A} + \underline{T}^{A}_{M} + \underline{T}^{M}_{M}) | \phi_k \rangle . \tag{25}$$

The situation where M has only sites at the right side of the barrier is the case that we will discuss in the following section, so that the expression for the flux reduces to

$$\Phi(\psi_k) = \frac{4\pi t a^2}{h} \mathrm{Im} \sum_{n \in A} \langle \phi_k | \underline{T}^{A\dagger}_{A} \underline{G}^{\dagger} | 0,n \rangle \times \langle 1,n | \underline{G} (\underline{T}^{A}_{A} + \underline{T}^{A}_{M}) | \phi_k \rangle . \tag{26}$$

We now insert Eq. (12) for the barrier Green's functions and Eq. (22) for the T matrix, and furthermore exploit the properties of the Green's functions given in Eq. (14). After these insertions the final expression for the flux becomes

$$\Phi(\psi_k) = \frac{4\pi t a^2}{h} \mathrm{Im} \sum_{m,n,\mu,\nu} [\sin^2(k_x a) e^{i[k_y a(m-n)]} \times \Theta^{*\nu}_{n} \Delta^{\mu}_{\nu} \Theta^{m}_{\mu}] \tag{27}$$

with the definition

$$\Delta_{n,n'} \equiv \Gamma_{n,n'} + 2(\underline{\Omega}\,\underline{\Lambda}^{-1}\underline{\Omega}^{t})_{n,n'} - \left[\frac{E}{2t} - 2\right] \delta_{n,n'} - \tfrac{1}{2}\delta_{1,|n-n'|} . \tag{28}$$

Note that the two δ functions in Eq. (28) have zero contribution after carrying out the summations in Eq. (27). The only other ingredient that we need in the expression for the conductance is the evaluation of the integral over all angles of incidence in Eq. (2). The spin degenerate density of states per unit angle is

$$\frac{\partial^2 n}{\partial E \partial \alpha} = \frac{1}{4\pi^2 t a^2} \times \frac{ka}{\cos\alpha \sin(ka\cos\alpha) + \sin\alpha \sin(ka \sin\alpha)} , \tag{29}$$

where k and α are on the fixed-energy contour

$$E = 2t[2 - \cos(ka\cos\alpha) - \cos(ka\sin\alpha)] . \tag{30}$$

The angular integral can be expressed in terms of the previously defined matrix Γ by means of the change of variable $\phi = ka\sin\alpha$,

$$\begin{aligned} \int_{-\pi/2}^{\pi/2} \frac{\partial^2 n}{\partial E \partial \alpha} \sin^2(k_x a) \cos[k_y a(n-m)] d\alpha &= \frac{1}{2\pi^2 t a^2} \int_{0}^{\cos^{-1}(1-E/2t)} (1-\zeta^2)^{1/2} \cos[(n-m)\phi] d\phi \\ &= \frac{-1}{2\pi t a^2} \mathrm{Im}\Gamma^{n}_{m} . \end{aligned} \tag{31}$$

We can combine Eqs. (31) and (27), which yields the final expression for the conductance

$$G = \frac{2e^2}{h} \mathrm{Tr}[(\mathrm{Im}\underline{\Gamma}^{*})(\mathrm{Im}\underline{\Theta}^{*}\underline{\Delta}\,\underline{\Theta})] . \tag{32}$$

In Ref. 7 we consider the situation where H_M is absent. In that case, Θ and Δ are equal to Γ^{-1} and Γ, respectively, as can be seen from Eqs. (22) and (28), so that our formula for the conductance reduces to the simple result

$$G = \frac{2e^2}{h} \mathrm{Tr}[(\mathrm{Im}\underline{\Gamma}^{*})(\mathrm{Im}\underline{\Gamma}^{-1})] . \tag{33}$$

V. NUMERICAL RESULTS

We begin by discussing how the conductance is influenced by the choice of the lattice parameter relative to the Fermi wavelength. As the reader may have noticed, the final expressions Eq. (32) and (33) depend in the first place on the shape of the microstructure defined by the sets of lattice sites A and M, and in the second place on the parameter $E_F/(2t)$. The dependence on the latter is through the matrices Γ, Δ, and Ω which are defined in Eqs. (13) and (21). For practical purposes it is more convenient to think in terms of length scales rather than energy scales. As we will be mainly interested in the long-wavelength regime, we can identify λ_F as $2\pi a(t/E_F)^{1/2}$. For higher energies there is no well-defined Fermi wavelength, due to the noncircular shape of the Fermi surface. (In fact, for $E_F=4t$ the Fermi surface is lozenge-shaped.) It is perhaps illustrative to point out that in typical GaAs-based 2D electron gases the Fermi wavelength is about 400 Å, whereas the lattice spacing of the three-dimensional fcc crystal structure of GaAs equals 5.7 Å. So the lattice constant is about 1% of the Fermi wavelength in a typical experimental situation. This means that if we want to do a "realistic" calculation of the quantum ballistic conductance under experimental conditions, we have to use $a/\lambda_F=0.005$ as a parameter. In fact, we will see that appreciable influence of the finite lattice parameter only occurs for $a/\lambda_F>0.07$. We like to point out that for samples with higher electron densities our tight-binding method is probably more realistic than a free-electron approach, because we are able to model certain deviations of the band structure from the free-electron parabola.

In Fig. 2(a) we present a plot of the conductance versus constriction width for three different values of a/λ_F, calculated for a zero-length constriction with Eq. (33). We see that the influence of the finite lattice parameter is small in the entire range of the conductance as long as $a/\lambda_F<0.04$. It is interesting to note that the vertical positions of the points of inflection are at precise integer multiples of $2e^2/h$ for these values of a/λ_F. In Fig. 2(b) we present a different sort of plot, where we vary the Fermi energy from 0 to $4t$. The latter value corresponds to half filling of the tight-binding band, where the Fermi surface is lozenge-shaped. The result is shown for a constriction of the type depicted in Fig. 1 and with a width of four sites and a length of zero, four, and ten sites. Only in the case of $L=0$ are the points of inflection at exact multiple integers of $2e^2/h$; in the other cases, oscillations on the plateaux (especially the higher ones) inhibit full quantization. The rest of the discussion relates to the situation where anisotropy of the Fermi surface can be neglected.

For larger constriction widths the oscillations decay and the conductance approaches the linear behavior of a classical Sharvin point contact,[16] i.e., $G=(2e^2/h)(k_FW/\pi)$, where W is the constriction width. There is, however, a slight offset of about 0.26 $(2e^2/h)$, which indicates that the effective width of the orifice is reduced by about 13% of a Fermi wavelength due to diffraction. This also helps us better understand why the

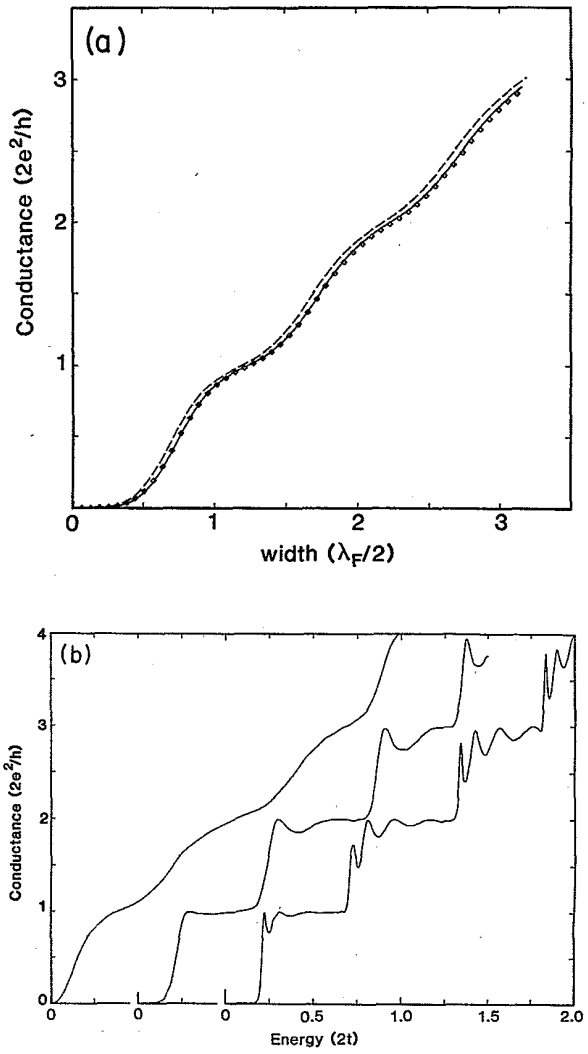

FIG. 2. (a) Conductance vs constriction width of a zero-length constriction for various values of the lattice parameter. Dashed curve, $a=0.0796\lambda_F$; lozenges, $a=0.0318\lambda_F$; solid curve, $a=0.0159\lambda_F$. (b) Conductance vs energy of constrictions with $W=4a$ and $L=0$, $4a$, and $10a$ from left to right.

conductance is pinched off for k_FW/π below about 0.25. The limit of very small constriction widths has been investigated by Rayleigh in a different context as early as 1897.[21] There have been numerous other theoretical investigations on wave propagation and diffraction throughout the first half of this century where the theory originated by Rayleigh has been further developed. A helpful review article covering most of the relevant literature has been published by Bouwkamp.[22] All of this work refers to propagation of electromagnetic and acoustic waves, which explains why the Fermi averaging required for the conductance is never carried out in these studies. We can nevertheless compare the exponent of the power-law behavior of the flux through a narrow aperture to classical results. Rayleigh has already pointed out that a narrow aperture acts as a radiating dipole source, which results in a $(kW)^4$ behavior of the

transmitted flux and a $\cos^2\alpha$ angular distribution of the transmitted intensity. In Fig. 3 we display a double-logarithmic plot of conductance versus constriction width for several values of ka. The solid line corresponds to $(kW)^4$, which agrees well with the curves for $ka=0.1$ and 0.2. For very low values of W the curve turns up again, but this is caused by the finite size of the lattice parameter, which is important if W and a are of the same order of magnitude. We now turn to the effect of constriction length on the shape of the conductance steps. A constriction of width W and length L can be modeled in the way displayed in Fig. 1. The matrix Γ is defined on the set of points A inside the aperture. The matrix Λ is on the set M of the pipe and Ω connects the sets A and M. With Eq. (32) we calculated several conductance-versus-length traces. In Fig. 4 we present some examples. The parameter a was $0.080\lambda_F$ in Fig. 4(a) and $0.032\lambda_F$ in Fig. 4(b). The larger value of the lattice parameter permits a larger range of the channel width, given the constraints on matrix size due to computational limitations. This is, however, at the expense of spatial resolution due to the discrete nature of a tight-binding lattice.

As seen in Fig. 4, plateaux develop very quickly on increasing the length of the constriction. In order to obtain more quantitative information we plot in Fig. 5 the data of Fig. 4 in a different way, i.e., as a plot of $\pi dG/d(kW)$ versus conductance. The minima correspond to the sections of minimal slope in Fig. 4. We checked that the horizontal positions of the minima correspond to multiples of $2e^2/h$ within numerical accuracy, which is better than 0.5%. We can study the development of plateaux by plotting the slope of the plateaux as a function of constriction length for each plateau index. The result is presented in Fig. 6. We see that the slope of each plateau decreases rapidly as function of constriction length. For

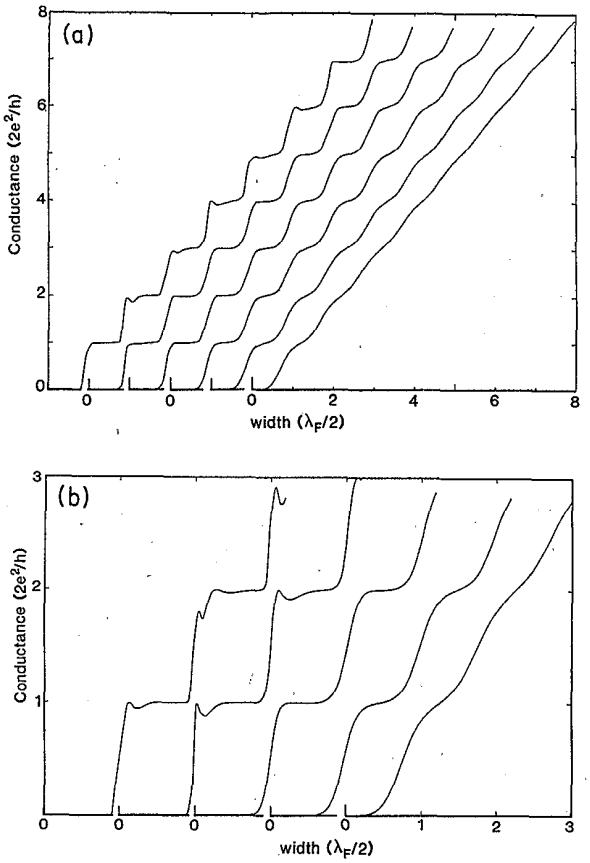

FIG. 4. (a) Conductance vs constriction width calculated for various constriction lengths, with $a=0.0796\lambda_F$. $L/\lambda_F=1.19$, 0.696, 0.478, 0.319, 0.159, and 0 from left to right. (b) The same as (a) with $a=0.0318\lambda_F$. $L/\lambda_F=1.592$, 0.987, 0.477, 0.255, and 0 from left to right.

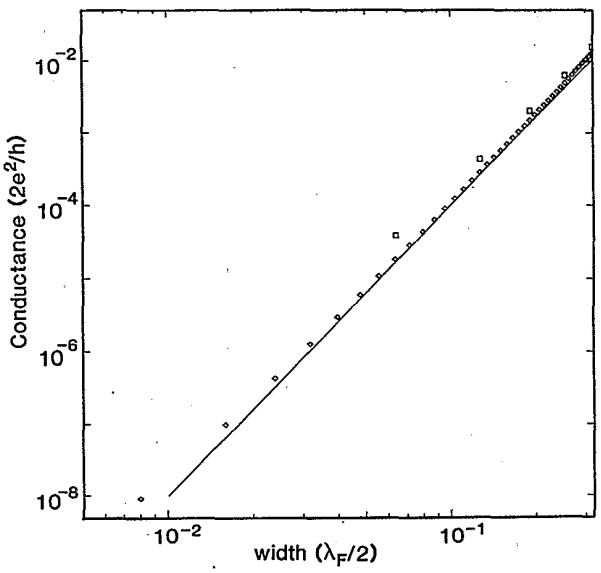

FIG. 3. Conductance vs constriction width on a log-log scale. Squares, $a=0.0318\lambda_F$; lozenges, $a=0.0159\lambda_F$; solid curve, $(kW)^4$.

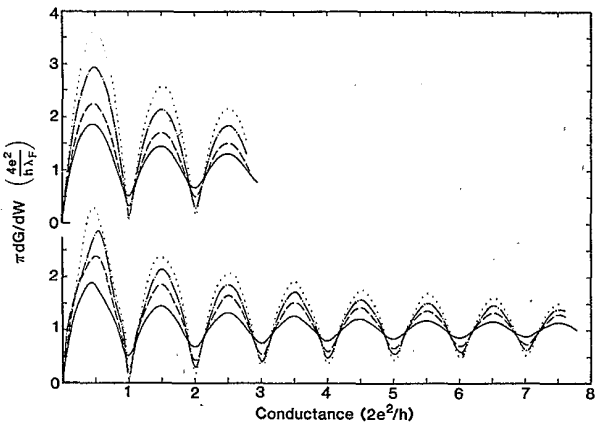

FIG. 5. $\pi\, dG/dW$ cs constriction width for channels of various length. Lower part: $a=0.796\lambda_F$. Solid, dashed, dash-dotted, and dotted curves: $L/\lambda_F=0$, 0.128, 0.255, and 0.350, respectively. Upper part: $a=0.0318\lambda_F$. Solid, dashed, dash-dotted, and dotted curves: $L/\lambda_F=0$, 0.159, 0.239, and 0.319, respectively.

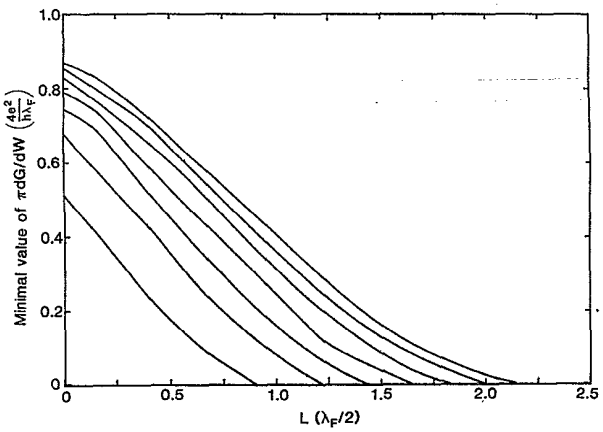

FIG. 6. The minimal values of dG/dW vs constriction length for the first seven plateaux. The plateau index increases from left to right.

the first seven steps a flat plateau is obtained for L smaller than the Fermi wavelength. Intuitively we might expect that a flat plateau should occur if the constriction is much longer than it is wide.[1] In fact, our calculations show that a much weaker constraint is sufficient. We can argue in the following way. For relatively short channels one has also to take into account the evanescent waves in the constriction, the decay length of which has to be long enough so that incoming waves on the left side can "tunnel" to outgoing waves on the right side. If the width of the channel is such that the Fermi level is in the nth subband of the constriction, the dominant contribution of evanescent waves comes from states tunneling below the $(n+1)$th subband. The decay length is given by

$$\kappa=\pi\left[\left[\frac{n+1}{W}\right]^2-\left[\frac{2}{\lambda_F}\right]^2\right]^{1/2}. \tag{34}$$

The minimal slope occurs at $k_F W/\pi\approx n+1/2$, so that

$$\kappa\approx\frac{2\pi}{\lambda_F}\left[\frac{\lambda_F}{2W}\left[1+\frac{\lambda_F}{8W}\right]\right]^{1/2}. \tag{35}$$

Tunneling can be neglected if κL exceeds a certain value. In other words, the nth plateau is flat for

$$\lambda_F\frac{2n+1}{(4n+3)^{1/2}}=cL\ , \tag{36}$$

where c is some constant. We can check from Fig. 6 that the values of L where the plateaux are horizontal indeed follow this behavior and that the constant c equals 3.16 within 2% accuracy. For sample dimensions large compared to λ_F this means that the condition for flat plateau is

$$L=0.32(2W\lambda_F)^{1/2}\ . \tag{37}$$

This is indeed a much weaker constraint than the intuitive assumption mentioned above. Taking the realistic parameters $\lambda_F=40$ nm and $L=100$ nm, we expect flat steps (apart from oscillations) for constriction widths up to 1.2 μm. This is a nice demonstration of the vitality of the concept of 1D channels, now widely used in studies of mesoscopic systems.[4,9,11,15] The steps can be washed out due to thermal smearing, of course; however, with the above parameters the energy difference between the highest subbands 60 and 61 of a constriction 1.2 μm wide is still of the order of 5 K. If the length of the constriction is increased beyond the point where the plateau becomes flat, oscillatory structure sets in. In Fig. 4(b) we show a plot of the first two plateaux for $L=0.987\lambda_F$ and $1.592\lambda_F$. These oscillations are due to the sharp edges at the ends of the constriction, which results in extra reflections on the left and right sides of the narrow region. Oscillations similar to those in Fig. 4(b) have been found experimentally for samples in the mK regime.[23] If the edges are very smooth, i.e., if the radius of curvature is much larger than λ_F, the coupling is called "adiabatic" and the oscillations disappear, as was shown by Glazman *et al.*[24] The necessity of adiabatic coupling in order to avoid reflections has also been pointed out by Landauer.[4] The oscillations can be qualitatively understood as follows: On increasing the width of the constriction the Fermi level crosses a sequence of 1D subbands. Hence with the Fermi level in the nth subband k_x increases from 0 to $\sqrt{2/n}\,k_F$ inside the narrow region, where the latter is the point where the $(n+1)$th step sets in. The transmission resonates with standing waves in the narrow region satisfying the soft boundary conditions on both sides of the constriction. This leads to an oscillation each time $k_x L$ approximately equals an integer multiple of π. This also implies that the number of oscillations on a plateau is proportional to L. Due to thermal smearing the oscillations will average out for constrictions beyond a certain temperature-dependent length.

The more or less regular oscillations due to reflections at the front and back ends of the constriction can also be regarded as a more general phenomenon, where reflections by irregularities both inside and outside the narrow region cause fluctuations on changing the constriction width. In the case of intermediate disorder one returns to the situation of a quasi-1D lead where universal conductance fluctuations occur on changing the phase relations of the wave functions at the Fermi level. This can, e.g., be accomplished by changing the channel width, the Fermi wavelength, or by applying a magnetic field.[9,25] Here we will only consider the situation of a constriction with a single impurity, which we believe is more relevant in the context of the present-day experiments on mesoscopic systems in high-mobility $GaAs/Al_xGa_{1-x}As$ 2D gases, as the elastic mean free path in those samples exceeds the constriction dimensions by at least an order of magnitude.

In Fig. 7 we present plots of the conductance versus constriction width in geometries where an impurity is added at several positions both inside and outside the narrow region. We make the following observations: If an impurity is positioned inside the narrow region, its effect is always to reduce the conductance and to suppress the steplike features. An impurity outside the constriction, however, can both enhance or suppress the conductance for certain widths. In all cases a delta-function impurity destroys quantization, i.e., either there

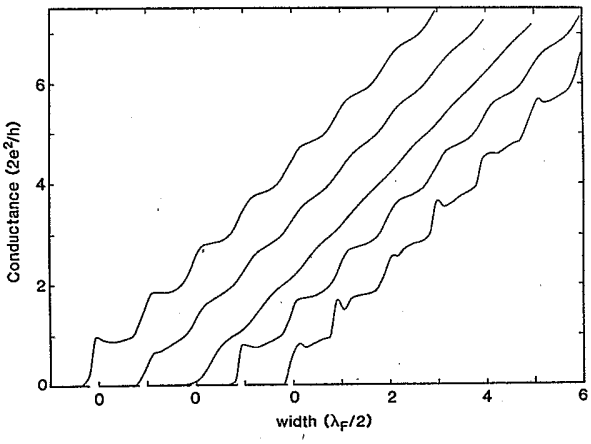

FIG. 7. Conductance vs constriction width calculated with $a=0.0796\lambda_F$ for several configurations involving a tube of length L and an impurity at position (X,Y). From left to right, $L/\lambda_F=0.0398$, 0.0398, 0.0398, 0.478, and 1.194 and $X/\lambda_F=0.71$, 0.56, 0.08, 0.22, and 0.43. Y equals $0.32\lambda_F$ for all curves.

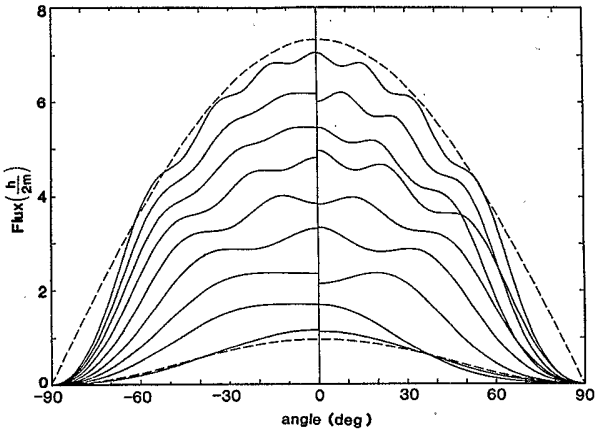

FIG. 8. Flux vs angle for a zero-length constriction (left panel) and a constriction of length $L=1.59\lambda_F$ and $a=0.0796\lambda_F$ (right panel). Dashed curves: $\cos^2\alpha$ (lower curve) and $\cos\alpha$ (upper curve). Solid curves, from top to bottom: $W/\lambda_F=3.7$, 3.3, 2.9, 2.5, 2.1, 1.3, 0.9, and 0.5 in both panels.

is additional structure on the plateaux, or the inflection points shift away from the quantized values quite drastically, regardless of the length of the constriction. In view of the oscillatory structures on the steps it is hard to define a good measure of the effect of an impurity. Our observation from calculations for various impurity positions is that the effect on the plateau position varies inversely proportional to the distance between the impurity and the constriction. More explicitly, δ-function impurity removed a distance λ_F from one of the ends of the constriction shifts the plateau by about 5% of $2e^2/h$. In high-purity samples, where the elastic mean free path is of the order of 5–10 μm, the typical distance between the constriction and the impurity would be of the order of a few micrometers, so that an upper limit for the precision of quantization would be approximately 0.1%. This more or less rules out possible applications as an alternative for the resistance standard based on the quantum Hall effect.

Finally, we discuss the diffraction pattern of a constriction averaged over all incoming Fermi wave vectors. We can use Eq. (27) to calculate $\Phi(\psi_k)$ as a function of angle of incidence. This is also the excess electron flux at the left side of the orifice due to a voltage drop where the right half-plane is at a higher (negative) voltage than the left half-plane. In Fig. 8 we display Φ versus exit angle for several values of the channel width, both for a channel of zero length and for a channel with $L/\lambda_F=1.59$. The oscillatory structure is of approximately equal strength in both cases. For very small widths the distribution follows a $\cos^2\alpha$ behavior, also indicated in the Fig. 8. This is consistent with classical wave mechanics.[21,22] For wide channels the overall pattern follows a $\cos\alpha$ behavior (dashed curve in Fig. 8), which is consistent with results for classical ballistic particles.[16] In the latter case there is additional structure, also for very wide constrictions. In fact, the number of oscillations is approximately equal to the number of steps at the width for which the diffraction pattern is calculated. This behavior can in principle be studied in a setup with two constrictions, where a magnetic field is used to move the diffraction pattern of one of the constrictions across the second one. Care has to be taken, however, to separate the diffraction pattern from classical electron focusing effects[26] as well as rapid oscillations due to the mode interference effects observed by van Houten *et al.*[27] and discussed by Beenakker *et al.*[28]

VI. CONCLUSIONS

We conclude that a straightforward tight-binding calculational scheme can be used to obtain numerically exact values of the conductance of a wide variety of microstructures in the quantum ballistic regime. We are able to calculate in detail the behavior of narrow constrictions, such as have been studied experimentally by van Wees *et al.*[1] and by Wharam *et al.*[2] This opens the possibility for predicting the behavior of new devices with a high degree of accuracy. As the preparation of submicrometer devices is a difficult and time-consuming task, feedback with numerically exact simulations will help to direct the research in a more efficient way. We find that steplike structures exist for surprisingly short channels, even down to zero length. The condition for flat steps is found to be that the constriction width W, the length L, and the Fermi wavelength λ_F have to satisfy $L=0.32(2W\lambda_F)^{1/2}$, which is more or less opposite to what one expects intuitively. The constriction is allowed to be much shorter than wide, rather than the other way around. For longer constrictions, extra oscillatory structure due to reflections destroys the quantization. The

presence of impurities also strongly affects the position of the steps, as well as their shape, regardless of the length of the constriction. Although conductance steps reasonably close to multiples of $2e^2/h$ are expected in very pure samples with optimized geometries, the zero-field conductance quantization effect is in principle unstable with respect to sample imperfections.

ACKNOWLEDGMENTS

We gratefully acknowledge B. J. van Wees, L. P. Kouwenhoven, C. J. P. M. Harmans, J. E. Mooij, and F. Hekking for stimulating discussions during the preparation of this paper and for thoroughly reading the manuscript.

[1]B. J. van Wees, H. van Houten, C. W. J. Beenakker, J. G. Williamson, L. P. Kouwenhoven, D. van der Marel, and C. T. Foxon, Phys. Rev. Lett. **60**, 848 (1988).

[2]D. A. Wharam, T. J. Thorton, R. Newbury, M. Pepper, H. Ajmed, J. E. F. Frost, D. G. Hasko, D. C. Peacock, D. A. Ritchie, and G. A. C. Jones, J. Phys. C **21**, L209 (1988).

[3]R. Landauer, IBM J. Res. Dev. 1, 233 (1957).

[4]R. Landauer, Z. Phys. B **68**, 217 (1987).

[5]D. S. Fisher and P. A. Lee, Phys. Rev. B **23**, 6851 (1981).

[6]P. W. Anderson, D. J. Thouless, E. Abrahams, and D. S. Fisher, Phys. Rev. B **22**, 3519 (1980).

[7]E. G. Haanappel and D. van der Marel, Phys. Rev. B (to be published).

[8]P. A. Lee and D. S. Fisher, Phys. Rev. Lett. **47**, 882 (1981).

[9]A. D. Stone, Phys. Rev. Lett. **54**, 2692 (1985).

[10]Y. Imry, in *Directions in Condensed Matter Physics, Memorial Volume in Honor of Shrangkeng Ma,* edited by G. Grinstein and G. Mazenko (World Scientific, Singapore, 1986), p. 101.

[11]M. Büttiker, Phys. Rev. B **33**, 3020 (1986); Phys. Rev. Lett. **57**, 1761 (1986).

[12]N. Garcia (unpublished).

[13]A. P. van Gelder (private communication).

[14]A. A. Lucas, H. Morawitz, G. R. Henry, J.-P. Vigneron, Ph. Lambin, P. H. Cutler, and T. E. Feuchtwang, Phys. Rev. B **37**, 10708 (1988).

[15]R. Landauer, Phys. Lett. 85A, 91 (1981); A. D. Stone and A. Szafer, IBM. J. Res. Dev. **32**, 384 (1988); R. Landuaer (unpublished).

[16]Yu. V. Sharvin, Zh. Eksp. Teor. Fiz. **48**, 984 (1965) [Sov. Phys.—JETP **21**, 655 (1965)].

[17]I. K. Yanson, Zh. Eksp. Teor. Fiz. **66**, 1035 (1974) [Sov. Phys.—JETP **39**, 506 (1974)].

[18]A. G. M. Jansen, A. P. van Gelder, and P. Wyder, J. Phys. C **13**, 6073 (1980).

[19]*Quantum Mechanics,* Vol. 3 of *Course of Theoretical Physics,* edited by L. D. Landau and E. M. Lifshitz (Pergamon, Oxford, 1965), p. 57.

[20]E. N. Economou, *Green's Functions in Quantum Physics* (Springer, Berlin, 1983).

[21]Lord Rayleigh, Philos. Mag. **43**, 259 (1897).

[22]C. J. Bouwkamp, Rep. Prog. Phys. **17**, 35 (1954).

[23]B. J. van Wees *et al.* (unpublished results).

[24]L. I. Glazman, G. B. Lesovick, D. E. Khmelnitskii, and R. I. Shekhter, Pis'ma Zh. Eksp. Teor. Fiz. **48**, 218 (1988).

[25]A. B. Fowler, A. Hartstein, and R. A. Webb, Phys. Rev. Lett. **48**, 196 (1982); C. P. Umbach, S. Washburn, R. B. Laibowitz, and R. A. Webb, Phys. Rev. B **30**, 4048 (1984).

[26]P. C. van Son, H. van Kempen, and P. Wyder, Phys. Rev. Lett. **58**, 1567 (1987).

[27]H. van Houten, B. J. van Wees, J. E. Mooij, C. W. J. Beenakker, J. G. Williamson, and C. T. Foxon, Europhys. Lett. **5**, 721 (1988).

[28]C. W. J. Beenakker, H. van Houten, and B. J. van Wees, Europhys. Lett. **7**, 359 (1988).